JOURNAL OF PROPULSION AND POWER
Vol. 20, No. 5, September–October 2004

Mixing and Combustion Studies Using Cavity-Based Flameholders in a Supersonic Flow

M. R. Gruber,* J. M. Donbar,† and C. D. Carter‡
U.S. Air Force Research Laboratory, Wright–Patterson Air Force Base, Ohio 45433
and
K.-Y. Hsu§
Innovative Scientific Solutions, Inc., Dayton, Ohio 45440

An experimental investigation of the mixing and combustion processes that occur in and around a cavity-based flameholder in a supersonic flow is reported. Cavity-based flameholders are commonly found in hydrocarbon-fueled scramjet combustors; however, detailed information concerning the behavior of these devices, their optimal shape and fueling strategies, combustion stability, and interactions with disturbances in the main airflow (i.e., shock trains or shock-boundary layer interactions) is largely unavailable in the existing literature. This work is part of an ongoing research program aimed at providing information to help fill these voids and improve the overall understanding of cavities for use as scramjet flameholders.

Nomenclature

D	=	cavity depth
L	=	cavity length
M	=	Mach number
P	=	static pressure
P_{inj}	=	injection pressure
T_0	=	stagnation temperature
x	=	streamwise position
y	=	transverse position
z	=	spanwise position
θ	=	cavity aft ramp angle

Introduction

DEVELOPMENT of hydrocarbon-fueled supersonic combustion ramjet (scramjet) engines is an active area of research around the world. Because of the inherent difficulties associated with hydrocarbon combustion in a high-speed flow (i.e., slow overall kinetic rates and very short combustor residence times), the need exists for development of robust flameholding schemes for use in these combustors. One candidate for such a flameholder is based on the wall cavity. Wall cavities are typically characterized as either open or closed. In an open cavity, the shear layer spans the entire cavity length, whereas a closed cavity is long enough for the shear layer to reattach to the bottom wall.[1] For scramjet applications where drag is a key consideration, open cavities are desirable because they impose a smaller drag penalty on the engine. Figure 1 illustrates the geometric features that describe a typical cavity flameholder. The length is defined as the distance from the cavity leading edge to the midpoint of the aft ramp.[2]

Received 22 September 2003; revision received 12 January 2004; accepted for publication 24 January 2004.

*Senior Aerospace Engineer, AFRL/PRAS Building 18, 1950 Fifth Street. Senior Member AIAA.
†Senior Aerospace Engineer, AFRL/PRAS Building 18, 1950 Fifth Street. Member AIAA.
‡Senior Aerospace Engineer, AFRL/PRAS Building 18, 1950 Fifth Street. Associate Fellow AIAA.
§Senior Research Scientist, 2766 Indian Ripple Road. Senior Member AIAA.

Several recent investigations have examined the utility of wall cavities as flameholders for liquid and gaseous hydrocarbon-fueled scramjet combustors.[1,3–11] In all cases, the cavity entrains oxidizer from the freestream. Fuel can be introduced into the cavity either by entrainment from the freestream (if fuel injection occurs upstream of the flameholder) or by direct injection. If sufficiently deep, the cavity offers a relatively long residence time for mixing and chemical reactions to take place.[12,13] Additionally, because the cavity is characterized by a relatively high recovery factor the total temperature of the mixture within the cavity is close to the total temperature of the freestream. Thus, if operated with a desirable fuel-air mixture favorable conditions are likely to exist within the flameholder for sustained combustion.

One key issue facing the design of a flameholder for hydrocarbon-fueled scramjets is the changing character of the flowfield depending on the operating mode of the combustor. Prior to ignition, the combustor flow is primarily supersonic. Assuming ignition takes place at a relatively low flight Mach number, the combustor is now typically characterized by dual-mode operation where a strong precombustion shock train exists. This system of shock waves creates a distorted flowfield containing regions of both supersonic and subsonic flow. As the vehicle accelerates to higher Mach numbers, the shock train weakens, and the flowfield through the engine returns to mainly supersonic. A robust flameholder must tolerate these flowfield changes without loss of effectiveness.

Previous Research at Air Force Research Laboratory

Mixing Measurements

The effectiveness of passive cavity fueling was examined in a nonreacting flow using the spontaneous vibrational Raman-scattering technique.[14] Ethylene was injected through a single circular injector located 35.6 mm upstream of a recessed cavity. The flush-wall injector (5.1 mm diam with injection angle of 15 deg) was placed on the spanwise centerline of the test section. The cavity ($D = 16.5$ mm, $L = 78.2$ mm, $\theta = 22.5$ deg) was recessed in a wall that diverged 2.2 deg from the horizontal. Fuel was introduced at two injection pressures, and the backpressure in the test section was varied from low (pure supersonic flow) to high (shock train present) using a control valve in the facility exhaust. Time-averaged Raman-scattering signals of ethylene and nitrogen were collected simultaneously at various transverse positions and several axial stations. These data were processed to obtain the cross-sectional distributions of equivalence ratio shown in Fig. 2. In these images, the flow direction is out of the page, and all axial positions are in millimeters. Also shown in this figure are two representative shadowgraph images

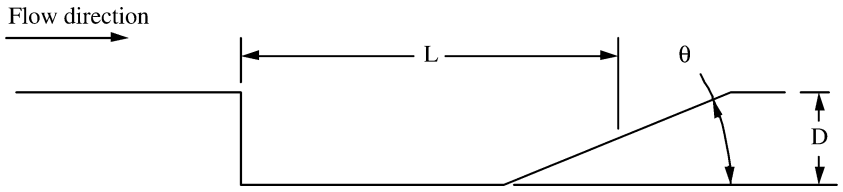

Fig. 1 General cavity geometry.

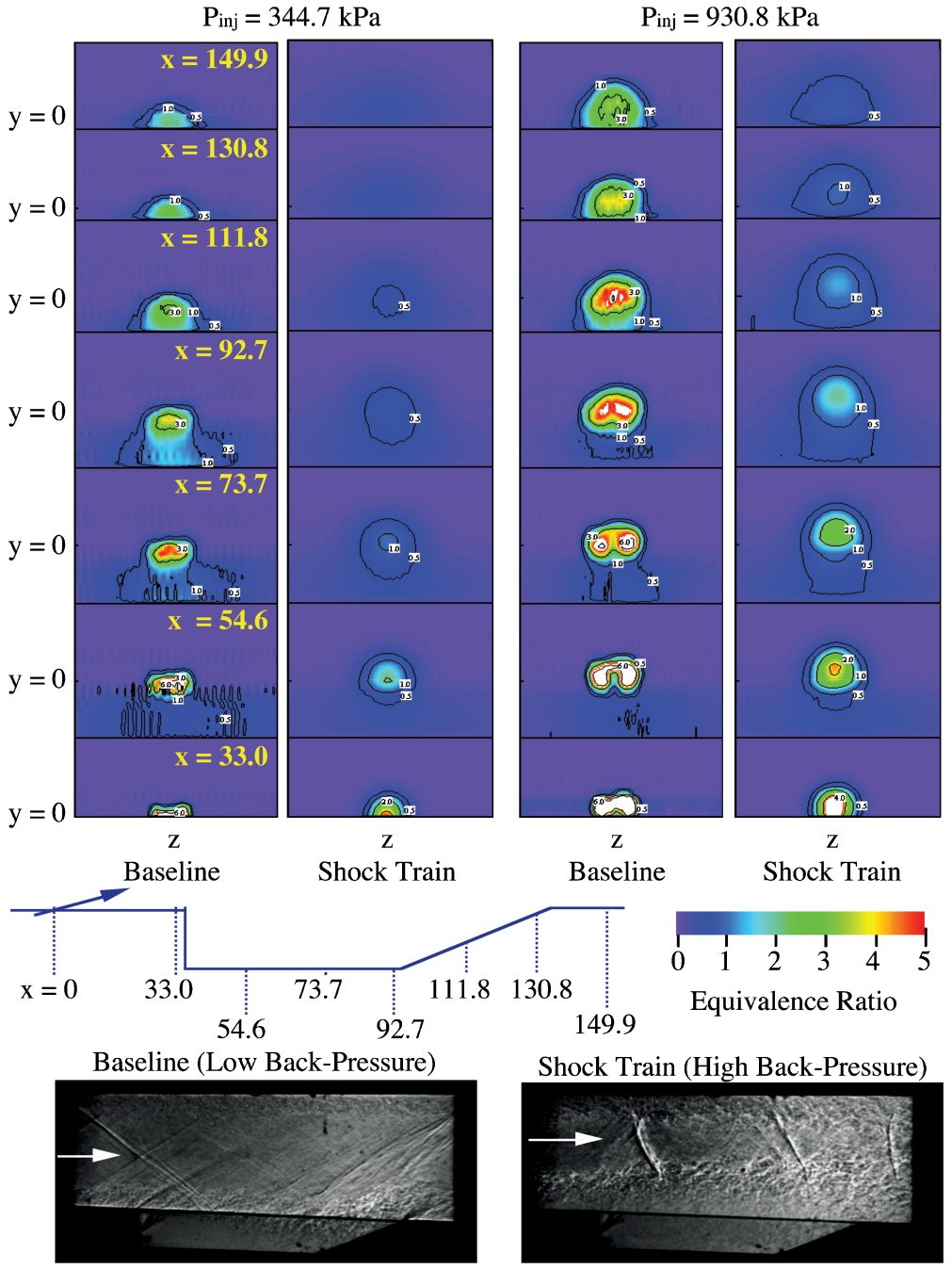

Fig. 2 Mixing of an ethylene jet in a clean and distorted supersonic flow.

(flow direction is left to right) that illustrate the flowfield with and without a shock train. The fuel plume penetrates higher into the main stream as the injection pressure is increased. Counter-rotating streamwise vortical structures are observed near the injector when the gas is injected into a clean supersonic flow (low backpressure). As the backpressure is increased, a normal shock train develops in the flow, leading to a highly distorted flowfield with boundary layer separation. As the fuel jet encounters this distorted flow, the fuel plume changes radically (see Shock Train columns in Fig. 2). The imposed shock system also elevates the fuel plume away from the wall, potentially affecting the stability of the flameholder by altering the entrainment of fuel and air into the cavity.

These results motivated two areas of investigation. First, to ensure stable cavity operation direct cavity fueling is proposed as a method for overcoming the transitional behavior encountered during the passive fueling study. Second, an instantaneous diagnostic is

of significant interest so that the mixing mechanisms can be better understood.

Combustion Measurements

To eliminate the influence of the cavity shear layer on the fuel distribution within the cavity, ethylene was directly introduced into the flameholder through a spanwise row of 10 injectors in the cavity ramp. Fuel was injected out of the aft ramp toward the rearward-facing step parallel to the cavity floor. A spark plug installed in the cavity floor facilitated ignition.

Flame chemiluminescent images of excited-state CH (CH*) and OH (OH*) were collected using two charge-coupled device (CCD) cameras positioned above the top quartz window of the test section. Separate color and interference filters were used for each camera to isolate the wavelength bands of interest. The CH* and OH* images were collected simultaneously with an exposure time of 0.2 s. Global cavity emission was measured using a GaP photodiode at a sampling rate of 10 kHz. The photodiode had an 11-mm^2 sensing area and spectral range of 245–405 nm. Signals from the photodiode were collected using a four-channel high-speed data-acquisition system.

Figure 3 shows the emission distributions of CH* and OH* over a range of fuel flow rates. Each image displays half of the cavity width extending from centerline to sidewall. Both CH* and OH* signals increase with fuel flow rate. At high fuel flow rates, flame emissions are distributed in a narrow region close to the cavity ramp with large spatial gradients. The emissions broaden to fill most of the cavity in the midrange of fuel flows. Further reductions in fuel flow rate cause reductions in the emission signal, revealing localized structures that eventually lead to lean blowout.

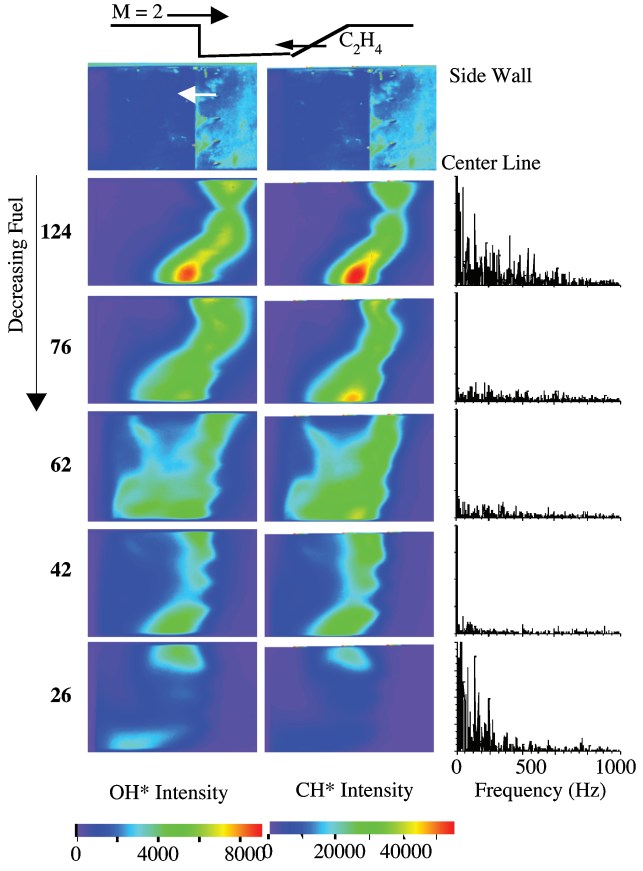

Fig. 3 Flame emission measurements at various ethylene flow rates standard liter per minute (SLPM).

The frequency spectra reduced from the GaP photodiode signal are also shown in Fig. 3. The emission fluctuations are higher at both high and low fuel loadings. The signal level is rather steady in the midrange of fuel flow when combustion fills the cavity volume most effectively. The localized emission structures observed in fuel-rich and fuel-lean conditions are correlated with the unsteadiness of cavity combustion. Dominant frequencies below 250 Hz were observed at low fuel loadings, whereas broadband high-frequency spectra were observed at higher fuel loadings. The low-frequency spectrum was caused by reignition of the distributed structures. These results motivate making instantaneous planar measurements in the reacting flowfield to learn more about the flame structure.

Current Work

The following sections describe recent efforts to obtain additional information about the fluid-mechanic and combustion characteristics of cavity-based flameholders in clean and distorted supersonic flows. Mixing studies examine the fuel distribution within and about the cavity using a variety of fuel-injection locations. Combustion studies (using ethylene as the fuel) characterize the reacting flowfield within and about the cavity and reveal the issues relevant to combustion stability. In both classes of experiments, advanced diagnostics play a vital role in improving the physical understanding of this important flowfield.

Experimental Facility

Test Facility

The facility used in this investigation was designed to allow basic studies of supersonic flows using conventional and nonintrusive diagnostic techniques. A continuous supply of clean compressed air is available to provide stagnation conditions up to 922 K and 2.8 MPa and a total maximum flow rate of 13.6 kg/s. A backpressure control valve positioned in the facility exhaust section allows remote control of the backpressure in the test section. Additional details describing the facility and its capabilities can be found elsewhere.[15]

A two-dimensional converging-diverging Mach 2 nozzle section, configured with an asymmetric nozzle, is used to develop the desired inlet conditions. The test section is connected directly to the 50.8 mm high by 152.4 mm wide exit of the facility nozzle. The test section has a constant-area isolator section (177.8 mm long), followed by a divergent ramp (2.5 deg over 740 mm in length). The modular cavity is flush mounted to the ramp in the divergent section. The cavity, shown in Fig. 4, is recessed from the surface with a 90-deg rearward-facing step, and the trailing edge is configured with a 22.5-deg ramp.

The current flameholder configuration has a depth of 16.5 mm and a length of 66 mm. Several fuel-injection locations were placed about the cavity as shown in Fig. 4; these locations are named F1, F2, F3, F4, and F5; details of these sites are listed in Table 1. Station F1 and F2 are inclined at 15 deg above the divergent wall. Stations F3

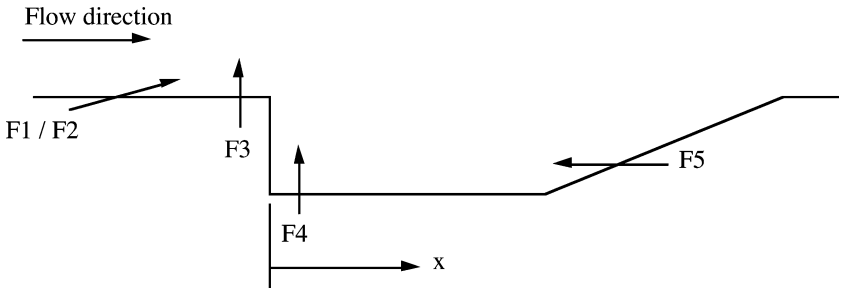

Fig. 4 Fueling options in present study.

and F4 consist of injector arrays oriented perpendicular to the wall. Finally, station F5 is placed in the 22.5-deg ramp 5.1 mm above the cavity floor. These injectors are directed parallel to the cavity floor.

Fuel-Injection System

The gas-injection system was automated and interfaced via a computer. The injection pressure was regulated with a dome loader and controlled remotely with an air-actuated isolation valve. The mass flow rate of gas was measured using a bank of Tylan mass flow controllers. A pressure transducer and thermocouple were used to measure the pressure and temperature of the injectant. All data were recorded in a computer for future analysis.

Planar Laser-Induced Fluorescence (PLIF) Diagnostics

Instantaneous measurements of the mixing and reacting flowfields were obtained using planar laser-induced fluorescence of nitric oxide (NO) and the hydroxyl radical (OH), respectively. In the NO-PLIF technique, a supply of air seeded with between 500 and 2000 ppm of nitric oxide was injected either into the Mach 2 freestream (passive fueling) or into the cavity flameholder (direct fueling). The OH-PLIF technique relied on the presence of the hydroxyl radical in the reacting flow experiments.

For both NO- and OH-PLIF, a Lumonics Hyperdye dye laser was pumped with the second harmonic of an injection-seeded Spectra Physics Nd:YAG laser (GCR-170). The dye laser output was frequency doubled using an Inrad Autotraker III. To generate the wavelength for NO excitation, a second Autotraker III was employed where the doubled-dye beam was frequency mixed with the residual infrared beam from the Nd:YAG. For NO excitation, the dye laser was set to a wavelength of 574 nm to produce frequency-mixed radiation at 226 nm to couple to the overlapped $Q_1(12)$ and $Q_2(20)$ transitions of the $A^2\Sigma^+ - X^2\Pi$ (0,0) band. For OH excitation, the dye laser was tuned to 587 nm so that the frequency-doubled radiation matched the wavelength for the $Q_1(8)$ transition of the $A^2\Sigma^+ - X^2\Pi$ (1,0) band. In both cases the resulting pump beam line width was $\sim 0.1\ \text{cm}^{-1}$. To ensure good overlap of the laser and transition, a portion of the UV beam was split off and directed over a small reference flame (and then to a fast photodiode); a simple set of lenses collected and focused the resulting LIF onto the photocathode of a photomultiplier tube. This signal, along with the photodiode output, was continuously displayed on an oscilloscope, allowing minor adjustments to be made to the dye laser grating position to mitigate the effects of test cell temperature changes.

The laser sheet was formed using a pair of lenses, a plano-concave cylindrical lens (−150-mm focal length) and a plano-convex spherical lens (1000-mm focal length). This arrangement resulted in a sheet height of about 50 mm. This sheet was directed across the span of the test section (through fused silica windows), and the resulting fluorescence was imaged off axis (to the sheet normal). This arrangement results in both image blur and distortion. Image blur was effectively mitigated by binning the pixels 3×3, resulting in an array size of 170×170 elements. No effort was made to correct the image distortion. The transmitting and receiving optical hardware were positioned on a traversing table allowing remote positioning of the measurement volume at any desired station in the flowfield.

A Princeton Instruments PIMAX CCD camera (512×512 pixel array) was used to detect the fluorescence. The camera was fitted with a UV lens (either a 105-mm focal length UV-Nikkor or a 45-mm focal length Cerco lens) and Schott glass filters. For OH LIF detection, fluorescence from the A-X(0,0) and (1,1) bands was isolated using UG-11 and WG-295 filters; for NO LIF detection, a UG-5 filter blocked scattering at 226 nm (as well as fluorescence from the (0,0) band) and collect fluorescence from the (0,1), (0,2), (0,3)... bands. The LIF images were not corrected for variations in line broadening, electronic quenching, or ground state population.

Table 1 Cavity fueling configuration

Injection site	Diameter, mm	Number of injectors	Axial location, mm	Lateral spacing, mm
F1	3.2	2	−25.4	22.9
F2	3.2	2	−25.4	38.1
F3	1.6	5	−5.1	25.4
F4	1.6	4	5.1	25.4
F5	1.6	10	58.4	12.7

Results and Discussion

Figure 5 illustrates the image plane orientation that applies to all of the fluorescence images presented in this section. As shown, the image plane is positioned at the cavity leading edge ($x = 0$). It extends from the Mach 2 freestream above the cavity down to the cavity floor. In each set of results to follow, all dimensions are in millimeters, and the flow direction is out of the page toward the reader's right (as indicated in Fig. 5). White lines in the images indicate the positions of the test section walls. At each axial position, 100 instantaneous images were collected. All images shown in this section correspond to a plane approximately 76.2 mm square. Figure 6 shows sample wall-pressure distributions for each back-pressure condition set during the mixing study.

Mixing Study

Passive Cavity Fueling

Figure 7 shows instantaneous NO images from selected axial locations for schemes F1 and F2. The jet structures are very dynamic

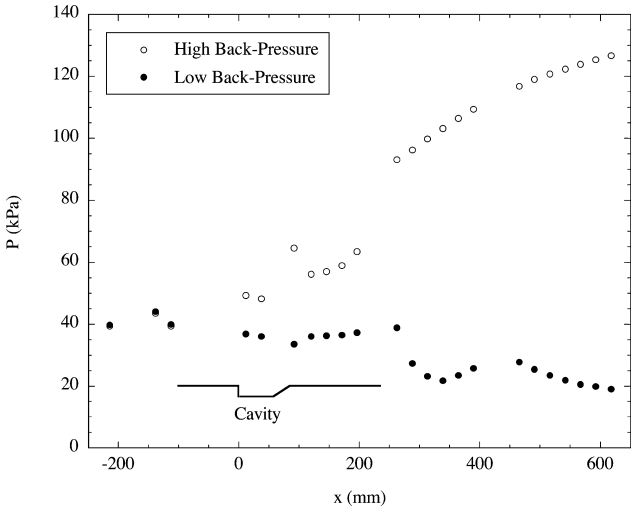

Fig. 6 Sample wall-pressure distributions used in mixing study.

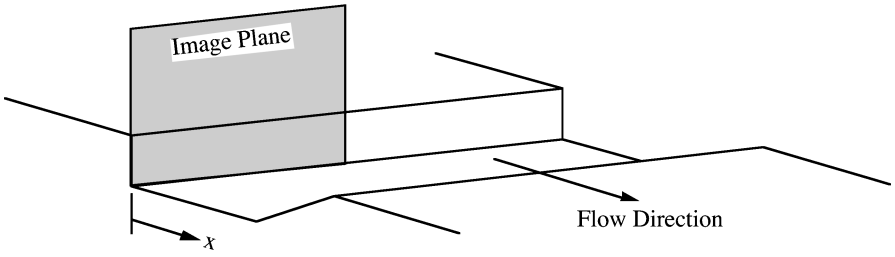

Fig. 5 Schematic illustrating the fluorescence image plane orientation.

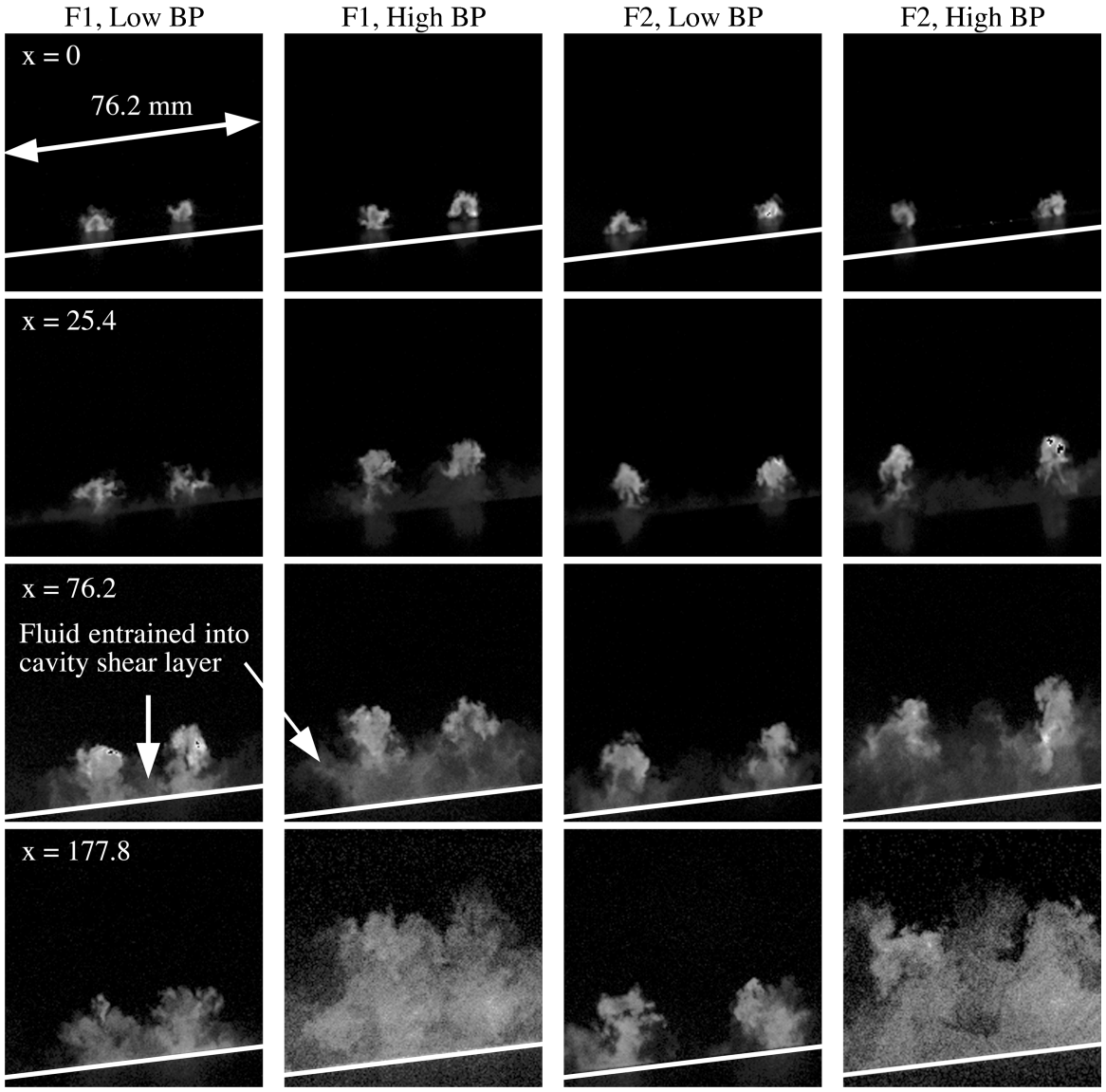

Fig. 7 Instantaneous NO-PLIF images; F1 and F2 (380 SLPM).

and vary from shot to shot. Each jet behaves similarly for both injector configurations. The plume penetration height increased with injection pressure, but the increase of plume height was only observed within the initial 76.2 mm. A region of low NO concentration between jets is observed in the cavity region ($x = 76.2$). This region is the result of recirculation of fluid containing NO that has been entrained into the shear layer. Only a small portion of injectant is entrained into the cavity, and this entrainment is inversely related to the jet penetration. As the backpressure increases, the shock-boundary-layer and shock-jet interactions dramatically enhance the mixing process. The jet penetration height and mixing in all directions are clearly illustrated in Fig. 7 at all stations. The axial length required for jet merging increases with the jet lateral spacing; however, the shock-train significantly reduces the merging length.

Figure 8 shows the ensemble-averaged (EA) and standard-deviation (SD) images from several axial locations for scheme F1. Each image results from processing the 100-image ensemble with corresponding background subtractions. Clearly, the jet plume grows downstream as it mixes with surrounding air. The highest fluctuations (and therefore most rapid jet mixing) occurred around the perimeter of the jet plume, as indicated in standard deviation images. Under higher backpressure, the jets lift toward the main flow. Similar observations exist for the F2 scheme.

Direct Cavity Fueling

Three injection schemes (F3, F4, and F5) were selected for the study of direct cavity fueling. Figure 9 shows the results from upstream injection (F3). In this scheme, the jets remain distinct above the cavity shear layer. A small fraction of NO is diluted and transported into the cavity. As the backpressure is increased, the jets penetrate higher into the mainstream, further reducing the cavity fueling. One can increase the cavity fueling by reducing the injection pressure; however, the fuel transport into the cavity still relies largely on diffusion through the shear layer and the shear layer's interaction with the cavity aft ramp. The effects of shock-boundary-layer interactions further complicate the entrainment process associated with F3 injection.

Figure 10 shows NO distributions at various axial locations within the cavity associated with injection through F4. High fluctuations are observed in the shear-layer region for both backpressure conditions as the jets interact with the shear layer. Besides the dynamic features of the jets, some large structures (indicated by distinct nonuniform NO distributions) appear in the cavity region, especially near the cavity leading edge. The nonuniform cavity fuel distribution is thought to be a result of secondary flow structures in the cavity that form in the corner between the leading edge and the side wall. This injection scheme seems to improve the cavity fueling as compared with upstream injection. However, cavity fueling continues to rely on the shear-layer interaction with the cavity aft ramp.

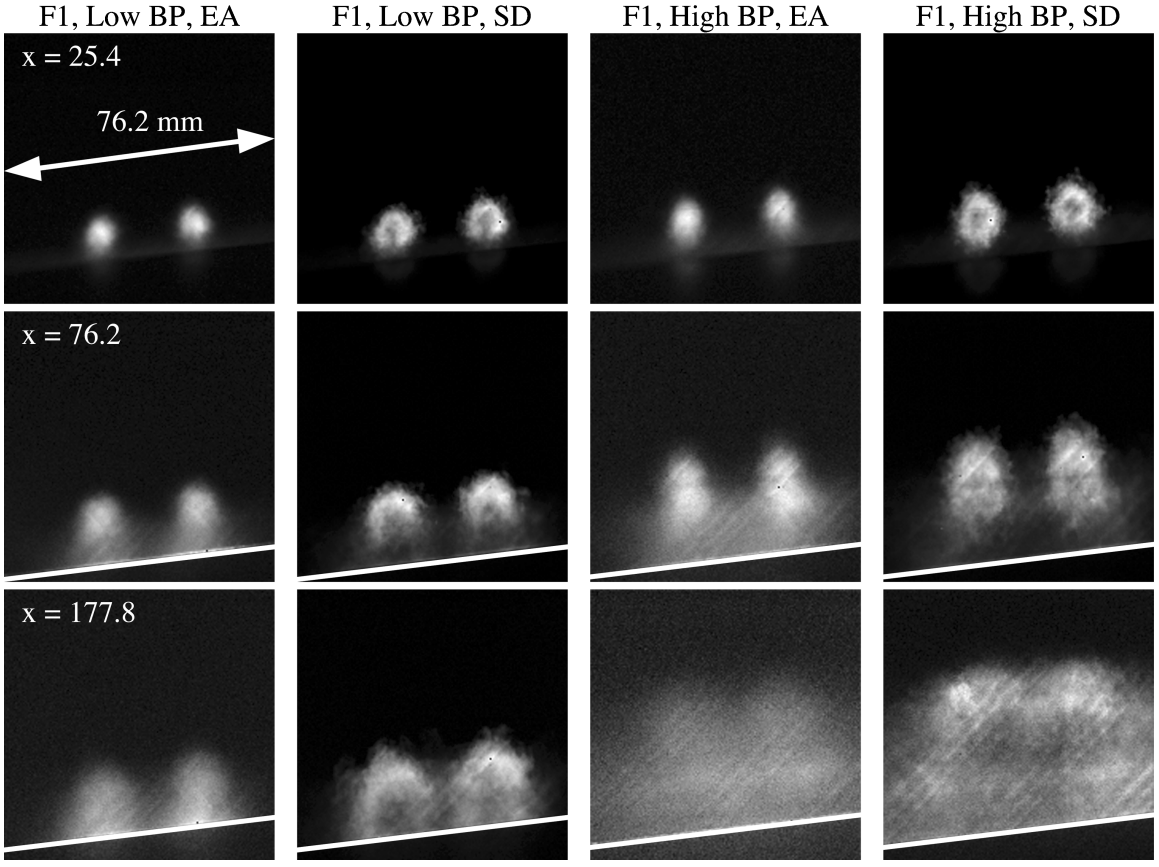

Fig. 8 Ensemble-averaged (EA) and standard-deviation (SD) images; F1 (380 SLPM).

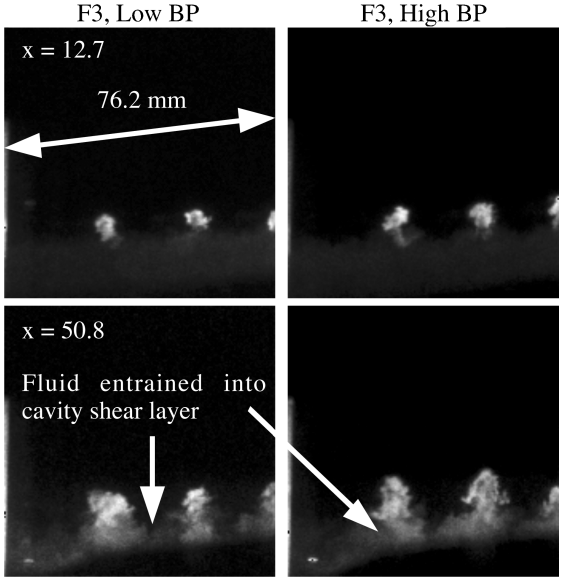

Fig. 9 Instantaneous NO-PLIF images; F3 (265 SLPM).

Finally, fuel is introduced from the cavity aft ramp through F5. With this scheme, the fuel distribution in the cavity becomes uniform as shown in Fig. 11. The mixture inside the cavity is mostly uniform as a result of increased residence time for mixing along the cavity floor. The reduction of fluctuations in the shear-layer region is further evidence of the effectiveness of this injection scheme. As the backpressure increases, the NO intensity decreases as a result of dilution with higher density air being entrained into cavity. A slight nonuniformity is observed in the corner region between

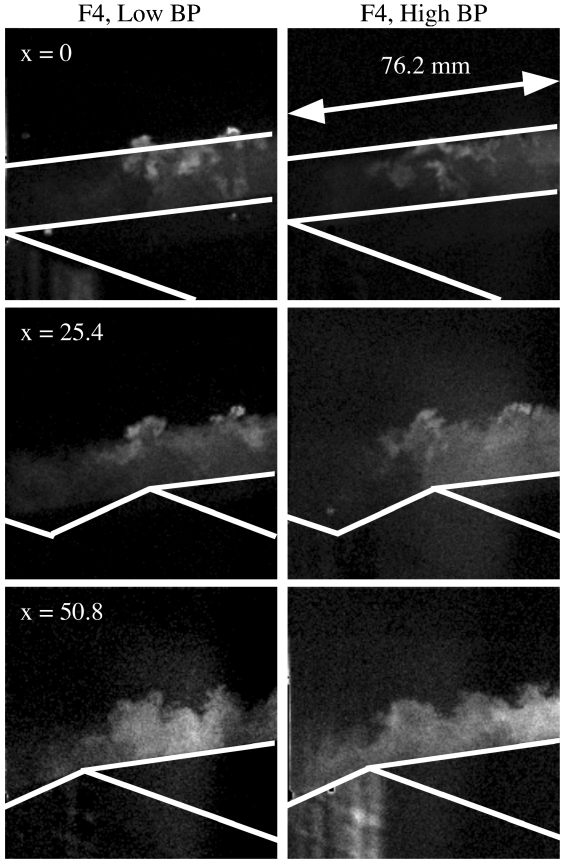

Fig. 10 Instantaneous NO-PLIF images; F4 (160 SLPM).

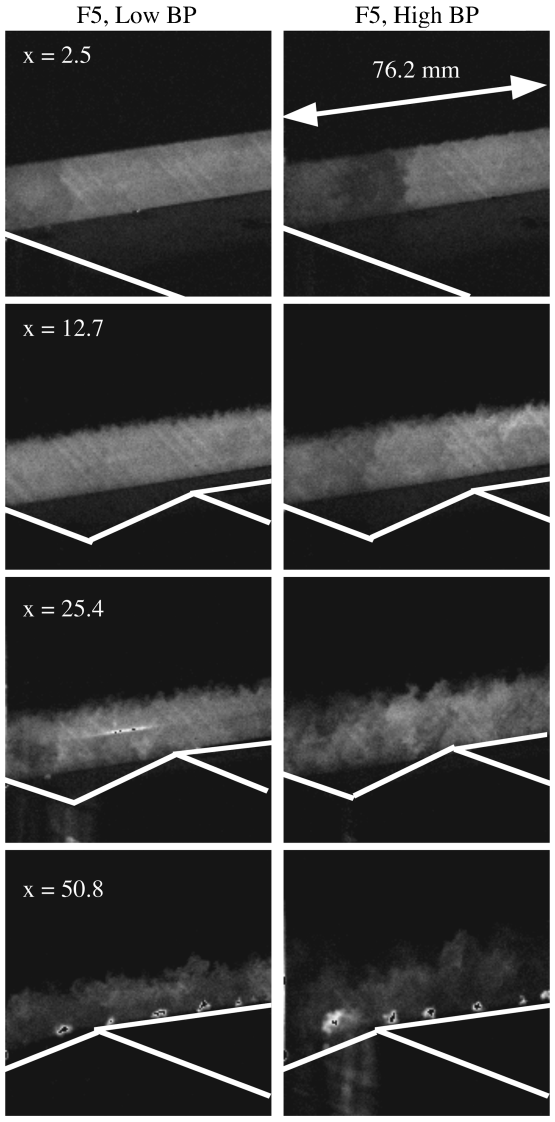

Fig. 11 Instantaneous NO-PLIF images; F5 (160 SLPM).

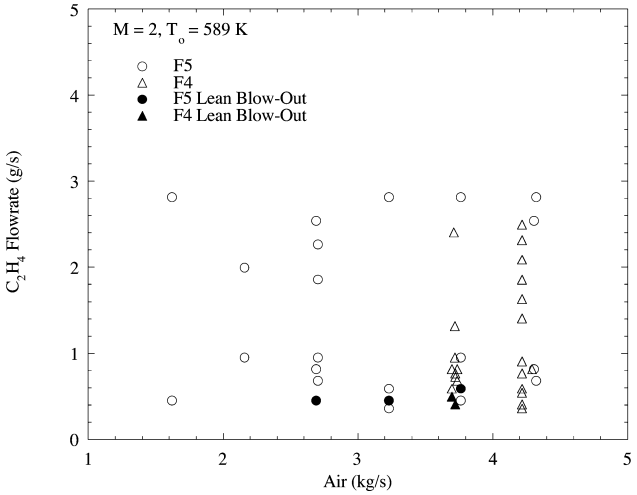

Fig. 12 Cavity flameholder operating characteristics.

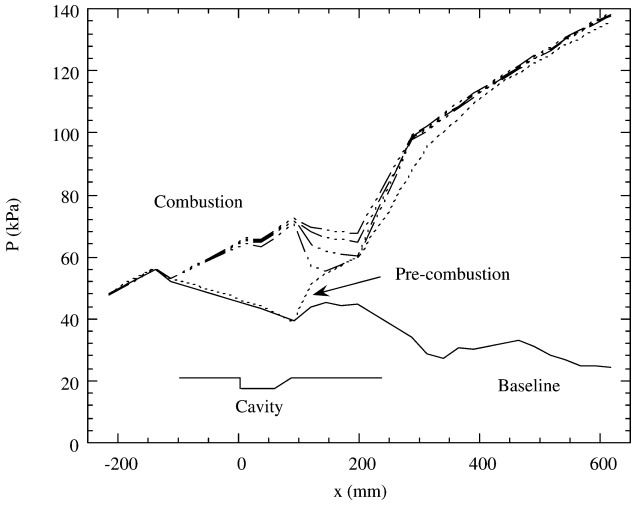

Fig. 13 Cavity ignition transient.

cavity leading edge and side walls. The secondary flow in this region is believed to be the reason of nonuniformity in mixing. The role of this secondary flow region becomes more evident at high backpressures. In general, increased backpressure has no significant effect on cavity fuel distribution except in the corner region and in the shear-layer region, where structures appear to be larger.

The nitric oxide used in the mixing study is not consumed. Any nitric oxide that is present in the cavity for a given laser pulse and is not transported out before the subsequent laser pulse will be imaged twice. This could lead to biased interpretations of mixing uniformity.

Combustion Study

Operating Range and Blowout Characteristics

Cavity combustion tests using ethylene were conducted at $M = 2$ with various freestream total pressures to establish the operation range for different cavity injection schemes (F3, F4, and F5). Total pressure varied between 206.8 to 551.6 kPa with air total temperature set to 589 K. A single spark plug located in the cavity floor was used for ignition. As the airflow reached the desired condition, the spark plug was energized, and ethylene was introduced through the desired fueling site. The spark plug was then turned off after the cavity flame was established.

Figure 12 shows all of the conditions for sustained cavity combustion where the flame sustained itself after the ignition source was deactivated. Adjusting the freestream total pressure varied the total air mass flow through the test section. For upstream injection (F3), cavity combustion could not be sustained over the conditions tested. Sustained combustion was observed at high P_0 when the cavity was fueled via F4. An online mass spectrometer was used to analyze gas samples collected from the wall just downstream of the cavity. The concentrations of H_2O, CO_2, and unburned C_2H_4 increase proportionally to the decrease of O_2 as the fuel flow rate increases. This clearly shows the fuel spillage through the shear layer and the limit of fuel consumption in a fixed volume cavity where air entrainment is relatively constant. A wider range of sustained flames was established using cavity ramp injection (F5). The upper limit of the fuel loading was restricted by the flow meters for these experiments. Limited lean blowout limits were established as shown in Fig. 12.

Ideally, the flameholder should sustain combustion as the shock system moves over the cavity and into the isolator section during the ignition transient. Several cavity combustion tests were conducted during the transition from low to elevated backpressure conditions (simulating the ignition event in a dual-mode scramjet combustor). Figure 13 shows several pressure traces obtained during these transient tests. The baseline distribution is taken before the combustion test commences and represents the pressure distribution associated with the low backpressure condition. Because of the slow response of the facility backpressure valve, the shock system was carefully prepositioned just downstream of the cavity prior to cavity ignition (see the trace labeled “Pre-combustion”). Once positioned, any appreciable heat release in the test section would be sufficient to force the shock train to move forward of the cavity flameholder. The cavity combustion test was then initiated to identify whether sustained combustion could be established. Fueling from F3 and F4 did not

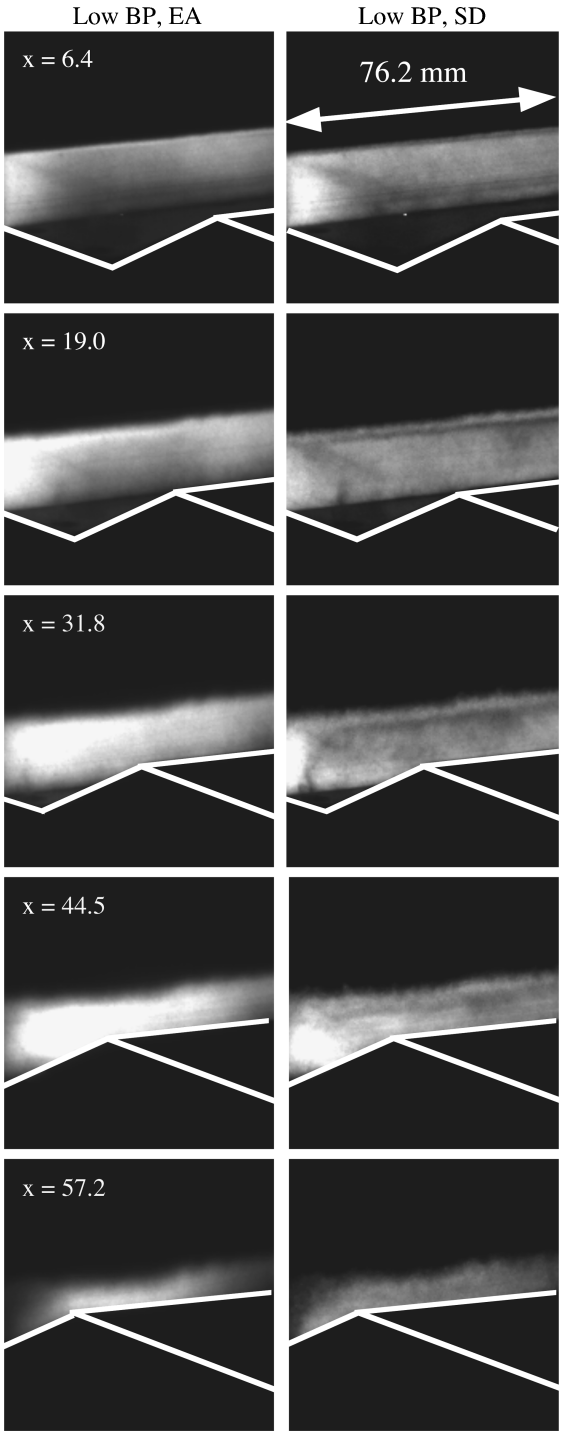

Fig. 14 EA and SD OH-PLIF images; F5 (40 SLPM).

result in sustained cavity combustion; as soon as the cavity was ignited, the shock system moved upstream of the cavity followed immediately by flame extinction. The shock system then moved back to its original position downstream of the flameholder. The only fueling scheme that produced sustained cavity combustion with the presence of the shock system was F5. As cavity ignition occurred, the shock system transitioned upstream of the cavity. Some oscillation in shock position was observed, but the flameholder stayed lit throughout. This result was consistent with the finding from the mixing study: the influence of the shock system and shear layer on cavity fueling is minimized by fuel injection from F5.

OH-PLIF Measurements

Planar distributions of the OH radical were collected at various axial locations within the cavity under different flow conditions. The

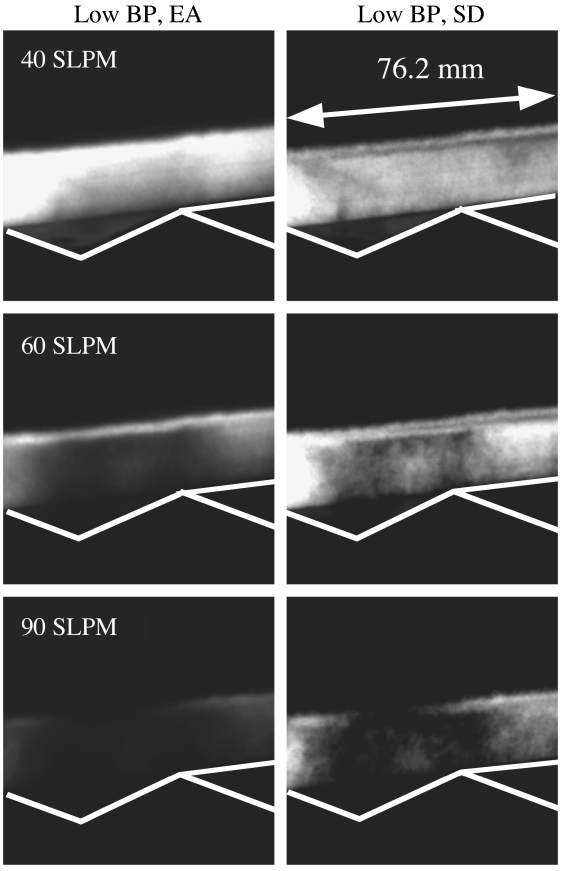

Fig. 15 EA and SD OH-PLIF images; F5 ($x = 19.0$).

cavity was fueled using station F5. EA and SD images obtained from 100 instantaneous OH images are shown in Fig. 14. Intense burning was found near the cavity ramp ($x = 44.5$), which is consistent with burn patterns observed on the hardware. High-intensity OH was also found in the corner region at the leading edge of cavity ($x = 6.4$) under this fuel loading. High fluctuations of distributed OH were observed in the leading portion of the cavity.

Figure 15 shows the sensitivity of the combustion zone to fuel flow rate at a given axial station. As the fuel flow rate increases from 40 to 60 SLPM, the fuel distribution in the upstream end of the cavity becomes nonuniform (as indicated by the dark regions in the center of the EA and SD images in Fig. 15). It is thought that this dark region is a fuel-rich lobe within the cavity (actually, there should be two—one on either side of the spanwise centerline). It is believed that his lobe structure forms aerodynamically as the freestream air interacts with the cavity. Because of the presence of this structure and its ability to retain fuel, the combustion zone becomes less uniform. At a fuel flow rate of 60 SLPM, combustion occurs as the rich mixture interacts with the shear layer. Further increases in fuel flow rate (to 90 SLPM) cause this lobe structure to become increasingly fuel rich (center regions in the images become darker), leading to the very poor combustion in the upstream end and nonuniform burning in the downstream portion of the cavity. The low-temperature fuel-rich region in the upstream portion of the cavity appears to inhibit the shear-layer flame from being ignited.

The influence of the shock system on cavity combustion is shown in Fig. 16 for a fuel flow rate of 90 SLPM. At this fuel loading, the combustion zone is dramatically altered by the shock train. Compared with the low backpressure case, the combustion zone in the high backpressure case fills more of the cavity volume and is more uniformly distributed. The shear-layer flame thickens and rises toward the crossflow. Recall that the shadowgraph image shown in Fig. 2 illustrates this lifting of the shear layer. It is expected that this process effectively increases the cavity volume allowing additional air to be entrained. This reduces the global fuel-air ratio within the

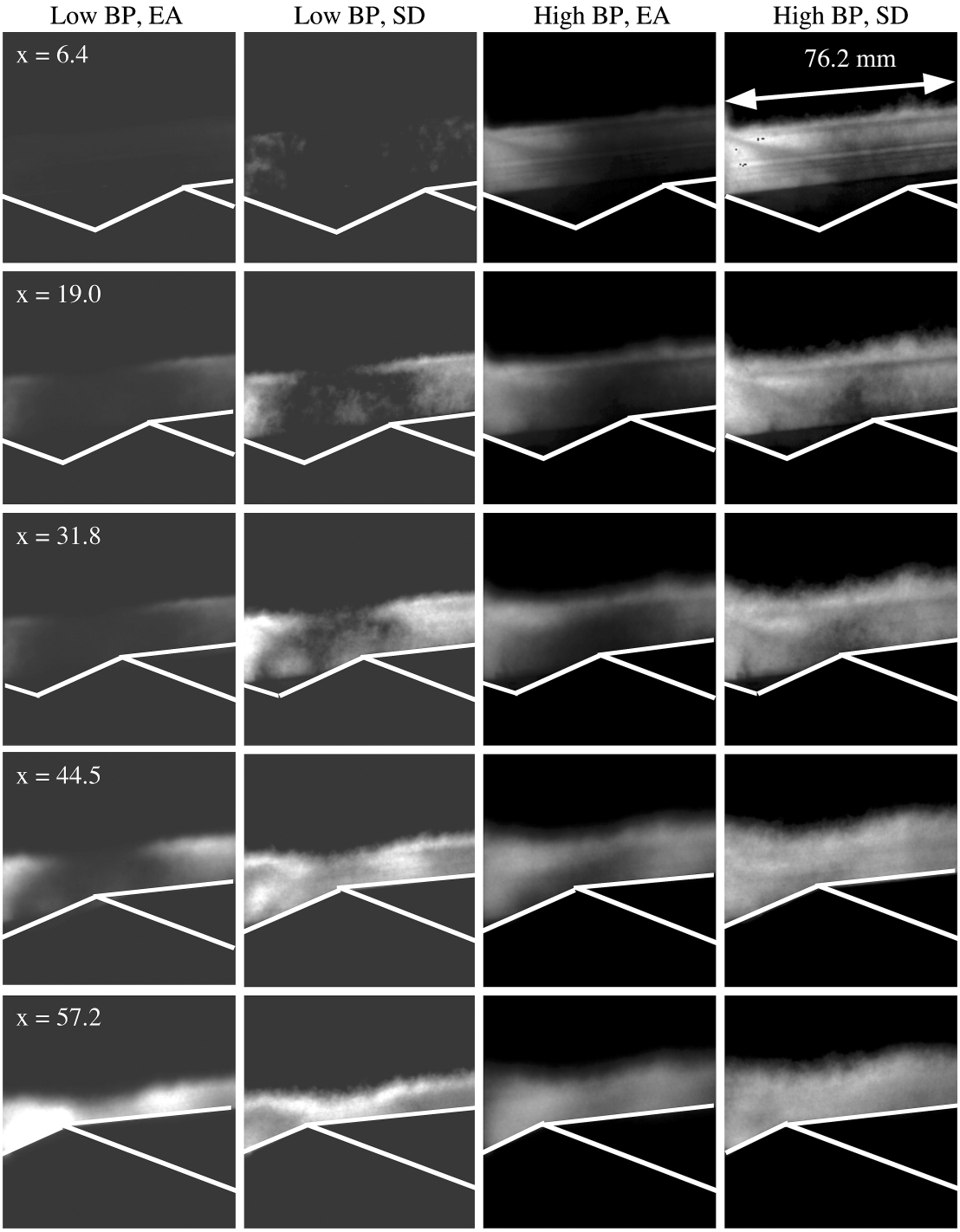

Fig. 16 EA and SD OH-PLIF images; F5 (90 SLPM).

cavity for a given fuel flow rate. It has also been shown that the shock train enhances the mixing within the cavity. Together, these two effects explain the improved volumetric efficiency and uniformity of the combustion zone within the cavity. The three-dimensional nature of the flowfield within the cavity appears to persist in the presence of the shock train: noticeable increases in the averaged OH signal and OH fluctuations are observed along the side-wall region.

Summary

Advanced diagnostic tools have been used to study the mixing and combustion processes that occur in typical cavity-based flameholders for supersonic combustion applications. These types of devices are commonly found in hydrocarbon-fueled scramjet combustor designs because they offer the benefits of relatively long residence time and high recovery factor accompanied by a moderate drag penalty. Robust flameholding will require the cavity to tolerate significant changes in the freestream flowfield of a dual-mode combustor without losing effectiveness. The current work highlights several observations regarding the importance of fuel-injection location on the transient stability of a typical cavity-based flameholder.

1) Passive entrainment of fuel from the main flow appears to be less desirable than direct cavity fuel injection for providing a spatially uniform fuel-air mixture and for maintaining a stable flame during the ignition transient.

2) Direct injection from the cavity ramp offers benefits over other methods of fuel injection, including a very uniform fuel-air

distribution within the cavity, a wide range of fuel flow rate over which cavity combustion can be sustained, and relative insensitivity to the flowfield changes that occur during the ignition event.

3) When the fuel flow rate into the cavity is properly tuned, minimum flame oscillations and maximum utilization of the cavity volume result. Deviations from this optimum level lead to a flame with increased oscillations and large spatial gradients.

4) An imposed shock train has a significant impact on the mixing and chemical reaction processes that occur in the cavity flameholder. This feature causes the cavity shear layer to separate, which effectively increases the volume of the cavity and the air entrainment. It also appears to enhance the mixing within the cavity volume, allowing more fuel to react.

Finally, the utility of flame emission sensors has been clearly shown. These devices allow rapid assessments of the flame character on both a time-averaged and instantaneous basis. The use of flame emission sensors as inputs to a fuel control system can offer significant benefits that allow optimization of the fuel distribution in the combustor over the vehicle flight trajectory.

Acknowledgments

This work was supported by the Air Force Office of Scientific Research under the guidance of Julian Tishkoff. The authors would like to acknowledge the contributions of K. Kirkendall, D. Schommer, and W. Terry for their technical support of this work. The support of the Research Air Facility is also appreciated.

References

[1]Ben-Yakar, A., and Hanson, R. K., "Cavity Flame-Holders for Ignition and Flame Stabilization in Scramjets: An Overview," *Journal of Propulsion and Power*, Vol. 17, No. 4, 2001, pp. 869–877.

[2]Gruber, M. R., Baurle, R. A., Mathur, T., and Hsu, K.-Y., "Fundamental Studies of Cavity-Based Flameholder Concepts for Supersonic Combustors," *Journal of Propulsion and Power*, Vol. 17, No. 1, 2001, pp. 146–153.

[3]Yu, K., Wilson, K. J., Smith, R. A., and Schadow, K. C., "Experimental Investigation on Dual-Purpose Cavity in Supersonic Reacting Flows," AIAA Paper 98-0723, Jan. 1998.

[4]Yu, G., Li, J. G., Chang, X. Y., Chen, L. H., and Sung, C. J., "Fuel Injection and Flame Stabilization in Liquid Hydrocarbon-Fueled Supersonic Combustors," *Journal of Propulsion and Power*, Vol. 19, No. 5, 2003, pp. 885–893.

[5]Yu, K. H., Wilson, K. J., and Schadow, K. C., "Effect of Flame-Holding Cavities on Supersonic Combustion Performance," *Journal of Propulsion and Power*, Vol. 17, No. 6, 2001, pp. 1287–1295.

[6]Mathur, T., Lin, K.-C., Kennedy, P. J., Gruber, M. R., Donbar, J. M., Jackson, T. A., and Billig, F. S., "Liquid JP-7 Combustion in a Scramjet Combustor," AIAA Paper 2000-3581, July 2000.

[7]Mathur, T., Gruber, M., Jackson, K., Donbar, J., Donaldson, W., Jackson, T., and Billig, F., "Supersonic Combustion Experiments with a Cavity-Based Fuel Injector," *Journal of Propulsion and Power*, Vol. 17, No. 6, 2001, pp. 1305–1312.

[8]Donbar, J. M., Gruber, M. R., Jackson, T. A., Carter, C. D., and Mathur, T., "OH Planar Laser-Induced Fluorescence Imaging in a Hydrocarbon-Fueled Scramjet Combustor," *The 28th International Symposium on Combustion*, The Combustion Institute, Pittsburgh, PA, Vol. 28, 2000, pp. 679–687.

[9]Gruber, M., Donbar, J., Jackson, T., Mathur, T., Eklund, D., and Billig, F., "Performance of an Aerodynamic Ramp Fuel Injector in a Scramjet Combustor," AIAA Paper 2000-3708, July 2000.

[10]Eklund, D. R., Baurle, R. A., and Gruber, M. R., "Numerical Study of a Scramjet Combustor Fueled by an Aerodynamic Ramp Injector in Dual-Mode Combustion," AIAA Paper 2001-0379, Jan. 2001.

[11]Baurle, R. A., and Eklund, D. R., "Analysis of Dual-Mode Hydrocarbon Scramjet Operation at Mach 4-6.5," *Journal of Propulsion and Power*, Vol. 18, No. 5, 2002, pp. 990–1002.

[12]Davis, D. L., and Bowersox, R. D. W., "Stirred Reactor Analysis of Cavity Flame-Holders for Scramjets," AIAA Paper 97-3274, July 1997.

[13]Baurle, R. A., Tam, C.-J., Edwards, J. R., and Hassan, H. A., "Hybrid Simulation Approach for Cavity Flows: Blending, Algorithm, and Boundary Treatment Issues," *AIAA Journal*, Vol. 41, No. 8, 2003, pp. 1463–1480.

[14]Hsu, K.-Y., Carter, C., Crafton, J., Gruber, M., Donbar, J., Mathur, T., Schommer, D., and Terry, W., "Fuel Distribution About a Cavity Flameholder in Supersonic Flow," AIAA Paper 2000-3585, July 2000.

[15]Gruber, M. R., and Nejad, A. S., "New Supersonic Combustion Research Facility," *Journal of Propulsion and Power*, Vol. 11, No. 5, 1995, pp. 1080–1083.